applied sciences

MDPI

Article

Ergodic Rate and Outage Performance of Full-Duplex NOMA Relaying with Channel Estimation Errors and Low-Resolution ADCs

Siye Wang *, **Yeqin Huang** and **Yong Yang**

School of Artificial Intelligence, Beijing University of Posts and Telecommunications, Beijing 100876, China
* Correspondence: wsy@bupt.edu.cn

Abstract: In this paper, we analyze the performance of a full-duplex (FD) cooperative non-orthogonal multiple access (C-NOMA) relaying system with an amplify-and-forward (AF) protocol in the presence of loopback interference in FD transceivers. Particularly, by considering channel estimation errors and quantization noise in low-resolution analog-to-digital converters (ADCs), the accurate approximation expression for the ergodic rate and closed-form solution for the outage probability are derived, respectively. The validity of the theoretical results is verified by Monte Carlo simulations, which show that both channel estimation errors and quantization noise have deleterious effects on ergodic rate and outage performance for moderate and high signal-to-noise ratios (SNR). In the second phase of the C-NOMA system, both the outage performance and ergodic sum rate decrease at high SNRs due to the effects of loop interference. When the ADC dynamic range reaches a certain level, the system performance is more affected by loopback interference and channel estimation errors compared to the quantization noise of the ADCs.

Keywords: full duplex; cooperative communication; non-orthogonal multiple access; channel estimation error; low-resolution ADC

check for updates

Citation: Wang, S.; Huang, Y.; Yang, Y. Ergodic Rate and Outage Performance of Full-Duplex NOMA Relaying with Channel Estimation Errors and Low-Resolution ADCs. *Appl. Sci.* **2023**, *13*, 6950. https://doi.org/10.3390/app13126950

Academic Editor: Dimitris Mourtzis

Received: 28 April 2023
Revised: 30 May 2023
Accepted: 3 June 2023
Published: 8 June 2023

1. Introduction

With the commercialization of fifth-generation (5G) wireless technology and the development of beyond-fifth-generation (B5G) and sixth-generation (6G) wireless technology, the introduction of various emerging high-capacity applications and the dramatic rise in the demand for and use of wireless data has put a huge burden on existing wireless networks. Non-orthogonal multiple access (NOMA) has been identified as a critical key technology in the next generations of wireless communications because of its ability to improve spectrum efficiency, reduce latency, and balance system throughput and user fairness [1]. Previously, traditional orthogonal multiple access (OMA) schemes, such as frequency division multiple access (FDMA), time division multiple access (TDMA), code division multiple access (CDMA), and orthogonal frequency division (OFDMA) were used for the air interface. The number of users served by these schemes is limited to the maximum number of available orthogonal resources. However, NOMA can be used to break the orthogonal resource limit and thus serve more users at the cost of increased receiver complexity [2].

NOMA technology introduces two domains, i.e., power-domain NOMA and code-domain NOMA. In a similar way to CDMA, code-domain NOMA is differentiated by assigning each user different codes, except that non-orthogonal time-frequency resources are used for transmission. In power-domain NOMA, different power levels are assigned to different users. Once received, the signal is decoded at the receiver using successive interference cancellation (SIC), which decodes each user's signal in turn according to its power level until the desired signal is obtained [3]. Although code-domain NOMA has better performance compared to power-domain NOMA, it requires more bandwidth and is more complex to implement. Cooperative relay is seen as a promising solution to effectively combat the shadowing effect in order to extend radio coverage while significantly increasing channel capacity. The signal-forwarding methods used by the relay nodes can be divided into amplify-and-forward (AF) and decode-and-forward (DF). Combining the technical advantages of cooperative relay and NOMA, cooperative NOMA (C-NOMA) is proposed to further improve transmission efficiency [4–6]. In [6], the performance of the NOMA system over Rician fading channels was investigated, and the expression of the average achievable rate was obtained.

The operation modes of transceivers can be divided into half-duplex (HD) and full-duplex (FD) modes. Conventional wireless communication systems often rely on HD operation, resulting in reduced resource utilisation. FD mode enables transceivers to simultaneously transmit and receive signals on the same frequency band, which has the potential to double the spectrum efficiency and is considered a promising technology for application in the next generation of wireless communication systems [7–9]. However, the excessive power difference between the device's own transmitted signal and the low-power received signal arriving from the remote transmit antenna generates loopback interference (LI) between the receiver and the transmitter. The LI causes the capacity of the FD system to be reduced to even less than the capacity of the HD system. Nevertheless, with the continuous development of interference cancellation chain technology consisting of an antenna domain, analogue circuit domain, and digital circuit domain, loopback interference can be suppressed to an acceptable range at the cost of increased receiver complexity [10,11]. In order to further improve the spectral efficiency of C-NOMA systems and reduce the time slot required for transmission, the use of FD mode has been proposed [12–15].

However, LI cancellation is implemented at the cost of increased hardware cost and power consumption, particularly as extra-high-resolution analogue-to-digital converters (ADCs) are required to avoid signal saturation before entering digital processing, which may not be desirable in practical system deployments. Several studies have focused on the impact of ADC quantization errors on system performance [16,17]. In practical communication scenarios, base stations or terminals use various methods, such as least squares (LS) estimation, minimum mean square error (MMSE) estimation, and even deep learning methods [18] to perform channel estimation in order to obtain channel state information (CSI) to select more efficient coding and modulation schemes to improve transmission performance. However, the Doppler shift and noise generated by the pilot signals used in the processing may lead to channel estimation errors. Some research has already studied the impact of channel uncertainty on system performance [19–22]. Ref. [19] studied the ergodic capacities of both FD and HD modes for two proposed scenarios. By considering channel estimation errors, closed-form expressions and accurate approximations of ergodic capacities for two scenarios were derived, respectively. Ref. [20] investigated the outage performance of FD and HD vehicle-to-vehicle networks over double-Rayleigh channels with channel estimation errors. Ref. [21] studied a coordinated direct and relay NOMA sytem. Closed-form expressions for the outage probabilities and ergodic rates were derived with imperfect channel state information and imperfect SIC. Ref. [22] studied uplink NOMA short-packet communications in the presence of hardware impairments and channel estimation errors with different decoding schemes. Closed-form expressions of the average BLER for the high SNR regime were derived.

Recently, the performance of FD C-NOMA systems has been investigated [23–26]. In [23], the authors analyzed the outage probability and sum rate of the FD NOMA system over Nakagami-*m* fading channels. Ref. [24] obtained analytical expressions for the outage probabilities experienced by the users and the system outage probability of FD C-NOMA with an energy-harvesting network under a time-switching relaying protocol. The exact analytical expression of the outage probability for FD C-NOMA with physical-layer network coding was derived in [25]. Ref. [26] studied an FD C-NOMA spectrum-sharing system and derived the analytical expressions for the outage probability and ergodic capacity. Furthermore, some existing studies have considered the impact of various non-ideal factors.

In [27], by considering the I/Q imbalance and an imperfect SIC, closed-form and approximate expressions for the outage probability and ergodic sum rate were derived. Ref. [21] investigated exact closed-form expressions for the outage probability and approximate closed-form expressions for the ergodic rates of the downlink users in the presence of an imperfect CSI and imperfect SIC. However, none of these studies considered the impact of ADC resolution and channel estimation errors on system performance.

In this paper, we will analyze the system performance under the existence of loopback interference, ADC quantization noise, and channel estimation errors with outage probability and ergodic rate as the main performance metrics. The contributions of this paper are as follows:

1. We consider a FD C-NOMA wireless communication system that uses an AF relay to assist in signal transmission between the base station and multiple users. The system performance analysis takes into account non-ideal conditions, such as LI caused by FD operation, channel estimation errors, and quantization errors generated by low-resolution ADCs.
2. We derive the theoretical expressions of the ergodic rate and outage probability for an FD C-NOMA multi-user system. Specifically, accurate approximate expressions of ergodic rate and closed-form solutions of the outage probability for each user are obtained by using the theories of order statistics and probability statistics.
3. We verify the mathematical results obtained through Monte Carlo simulations. For the C-NOMA relay network, we discuss the impact of base station transmission power, relay amplification, forwarding power, relay LI level, quantization error level, and channel estimation error level on system performance. Theoretical and simulation results demonstrate the feasibility of the proposed theoretical approach.

The rest of this paper is organized as follows. Section 2 introduces the system model of a multi-user FD C-NOMA relay network. In addition, the signal models include channel estimation errors, loop interference, and ADC quantization error. Sections 3 and 4 provide theoretical analysis for the system ergodic rate and outage probability, respectively. Section 5 shows the theoretical and simulation results of system performance metrics under different parameters. Finally, Section 6 concludes the paper.

Notations: We use $\mathcal{CN}$ to denote the complex normal distribution and i.i.d. to denote "independent and identically distributed". $\mathbb{E}(\cdot)$ denotes the expected value of random variables. $\Pr(\cdot)$ indicates the probability of an event.

2. System Model

The system model is shown in Figure 1, which depicts an FD C-NOMA relaying network consisting of one base station (S), one FD relay (R), and N pieces of user equipment (UEs). In this network, both the base station and each UE are equipped with a single antenna, while the relay is equipped with one isolate transmit and one isolated receive antenna. Each UE uses a low-resolution ADC for analog-to-digital conversion. We assume that all channels are Rayleigh fading and consider the existence of channel estimation errors. There are no direct links between the BS and UEs due to the obstruction of obstacles.

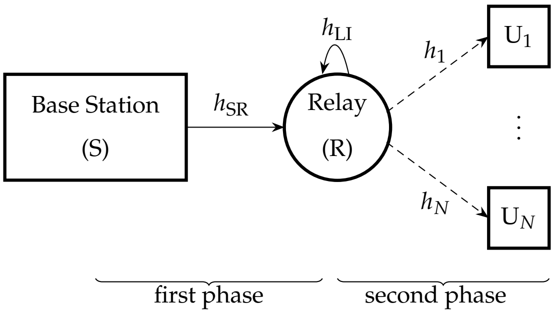

Figure 1. System model of FD C-NOMA relaying system without direct link.

Based on the NOMA protocol, we rearrange the N users according to the estimate of channel gains in the second phase. We denote $(\hat{h}_1, \cdots, \hat{h}_N)$ as the order statistic of $(\hat{h}_{\mathrm{RU}_1}, \cdots, \hat{h}_{\mathrm{RU}_N})$ in modulus. $|\hat{h}_n|$ is the nth-smallest value in $\{|\hat{h}_{\mathrm{RU}_1}|, \cdots, |\hat{h}_{\mathrm{RU}_N}|\}$. Then, we have $|\hat{h}_1| \leq \cdots \leq |\hat{h}_N|$. Here and in what follows, we shall denote the user corresponding to $\hat{h}_n$ as the nth user or user n ($n \in N$).

According to the channel estimation model of block fading in [20], we assume that all channels are quasi-static Rayleigh-fading channels. All the channels are assumed to be Rayleigh block-fading channels because the channel coefficients are constant on a block and they only change between each block. Each channel coefficient h is a sum of its estimate and the estimation error, which can be written as

$$h = \hat{h} + \epsilon_h, \tag{1}$$

where $\hat{h} \sim \mathcal{CN}(0, \sigma_h^2)$ is the estimate of the channel coefficient h and $\epsilon_h \sim \mathcal{CN}(0, \sigma_{\epsilon_h}^2)$ is the corresponding estimation error, assuming the channel estimate and estimation error are uncorrelated.

Let $h_{\mathrm{SR}} \sim \mathcal{CN}(0, \tilde{\beta}_{\mathrm{SR}})$ denotes the channel coefficient from S to R. $h_{\mathrm{RU}_n} \overset{\text{i.i.d}}{\sim} \mathcal{CN}(0, \tilde{\beta}_{\mathrm{RU}})$ denotes the independently identical distribution channel coefficients between R and N users. Then, we have

$$\begin{aligned} h_{\mathrm{SR}} &= \hat{h}_{\mathrm{SR}} + \epsilon_{\mathrm{SR}} \\ h_{\mathrm{RU}_n} &= \hat{h}_{\mathrm{RU}_n} + \epsilon_{\mathrm{RU}_n} \end{aligned} \tag{2}$$

where the channel estimation error term $\epsilon_{\mathrm{SR}} \sim \mathcal{CN}(0, \sigma_{\mathrm{SR}}^2)$ and $\epsilon_{\mathrm{RU}_n} \overset{\text{i.i.d}}{\sim} \mathcal{CN}(0, \sigma_{\mathrm{RU}}^2)$. Then, the channel coefficients can be expressed as $\hat{h}_{\mathrm{SR}} \sim \mathcal{CN}(0, \beta_{\mathrm{SR}})$, where $\beta_{\mathrm{SR}} = \tilde{\beta}_{\mathrm{SR}} - \sigma_{\mathrm{SR}}^2$ and $\hat{h}_{\mathrm{RU}_n} \overset{\text{i.i.d}}{\sim} \mathcal{CN}(0, \beta_{\mathrm{RU}})$, where $\beta_{\mathrm{RU}} = \tilde{\beta}_{\mathrm{RU}} - \sigma_{\mathrm{RU}}^2$. Here, we assume that the variables above in the first and second phases are mutually uncorrelated.

In the first phase, the base station transmits the superimposed signal to the relay. The transmit signal is denoted as

$$s_{\mathrm{S}} = \sqrt{P_{\mathrm{S}}} \sum_{n=1}^{N} \sqrt{a_n} x_n \tag{3}$$

where P_{S} is the transmission power at the base station S, a_n is the power allocation coefficient for user n, and x_n is the information signal transmitted to user n with unit energy, i.e., $\mathbb{E}|x_n|^2 = 1$, $n \in N$. The power coefficients are subjected to $\sum_{n=1}^{N} a_n = 1$ and $a_1 \geq \cdots \geq a_N$.

The received signal at relay S can be expressed as

$$r_{\mathrm{R}} = h_{\mathrm{SR}} s_{\mathrm{S}} + h_{\mathrm{LI}} s_{\mathrm{R}} + w_{\mathrm{R}} \tag{4}$$

where $w_{\mathrm{R}} \sim \mathcal{CN}(0, \sigma_{\mathrm{R}}^2)$ denotes the complex circularly symmetric additive white Gaussian noise (AWGN), and $h_{\mathrm{LI}} \sim \mathcal{CN}(0, \beta_{\mathrm{R}})$ is the residual LI coefficient after some interference cancellation methods.

In the second phase, the relay forwards the signal s_{R} with the AF protocol to N users $\mathrm{U}_1, \cdots, \mathrm{U}_N$. By the AF relaying, the relay amplifies the received signal by a factor A_{R} with a processing delay τ. The transmit signal s_{R} of the relay can be expressed as

$$s_{\mathrm{R}}[n] = \sqrt{P_{\mathrm{R}}} A_{\mathrm{R}} r_{\mathrm{R}}[n - \tau] \tag{5}$$

where P_{R} is the transmit power of the relay. The instantaneous transmit power of R should be P_{R}, which is shown as

$$\begin{aligned} P_{\mathrm{R}} &= \mathbb{E}|s_{\mathrm{R}}|^2 \\ &= P_{\mathrm{R}} A_{\mathrm{R}}^2 \mathbb{E}|r_{\mathrm{R}}|^2 \\ &= P_{\mathrm{R}} A_{\mathrm{R}}^2 \left(\mathbb{E}|h_{\mathrm{SR}}|^2 P_{\mathrm{S}} + \beta_R P_{\mathrm{R}} + \sigma_{\mathrm{R}}^2 \right) \end{aligned} \tag{6}$$

Hence, the amplification factor can be denoted as

$$A_{\mathrm{R}} = \frac{1}{\sqrt{P_{\mathrm{S}}|\hat{h}_{\mathrm{SR}}|^2 + P_{\mathrm{S}}\sigma_{\mathrm{SR}}^2 + P_{\mathrm{R}}\beta_{\mathrm{R}} + \sigma_{\mathrm{R}}^2}} \tag{7}$$

Then, the received signal at user U_n can be expressed as

$$r_n = h_n s_{\mathrm{R}} + w_n \tag{8}$$

where $w_n \sim \mathcal{CN}(0, \sigma_{\mathrm{U}}^2)$ denotes the AWGN at user n.

The signal received by the user is first fed to the ADC for processing with the quantization, as shown in Figure 2. As described in [17], the output of a low-resolution ADC corresponding to input $r_n(m)$ can be expressed as

$$\bar{r}_n(m) = \alpha r_n(m) + \bar{n}_r \tag{9}$$

where the values of α is determined by the quantization bits of the ADC, as illustrated in Table 1.

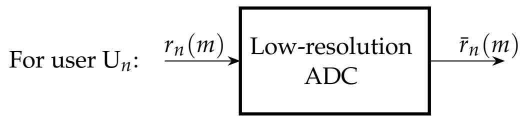

Figure 2. System model of low-resolution ADCs.

Let b be the number of quantization bits. When $b > 5$, the parameter α is given by

$$\alpha = 1 - \frac{\pi\sqrt{3}}{2} 2^{-2b} \tag{10}$$

and when the quantization bit $b \leq 5$, the value of α is given as follows:

Table 1. Values of the α parameter corresponding to different quantization bit numbers.

Quantization Bits	α
1	0.6366
2	0.8825
3	0.96546
4	0.990503
5	0.997501

$\bar{n}_r$ denotes the additive quantization noise, which has a complex normal distribution with zero mean and variance,

$$\mathbb{E}|\bar{n}_r|^2 = \alpha(1-\alpha)\mathbb{E}|r_n(m)|^2 \tag{11}$$

The power of the quantized signal obtained by the user n can be expressed as

$$\begin{aligned} \mathbb{E}|\bar{r}_n|^2 &= \mathbb{E}|\alpha r_n|^2 + \mathbb{E}|\bar{w}_n|^2 \\ &= \alpha^2 \mathbb{E}|r_n|^2 + \alpha(1-\alpha)\mathbb{E}|r_n|^2 \\ &= \alpha \mathbb{E}|r_n|^2 \end{aligned} \tag{12}$$

The quantized signal obtained by the user n is given by

$$
\begin{aligned}
\bar{r}_n &= \alpha r_n + \bar{n}_r \\
&= \alpha(h_n s_{\mathrm{R}} + w_n) + \bar{n}_r \\
&= \alpha(h_n \sqrt{P_{\mathrm{R}}} A_{\mathrm{R}} r_{\mathrm{R}} + w_n) + \bar{n}_r \\
&= \alpha[h_n \sqrt{P_{\mathrm{R}}} A_{\mathrm{R}} (h_{\mathrm{SR}} s_{\mathrm{S}} + h_{\mathrm{LI}} s_{\mathrm{R}} + w_{\mathrm{R}}) + w_n] + \bar{n}_r \\
&= \alpha\left[(\hat{h}_n + \epsilon_n)\sqrt{P_{\mathrm{R}}} A_{\mathrm{R}} ((\hat{h}_{\mathrm{SR}} + \epsilon_{\mathrm{SR}}) s_{\mathrm{S}} + h_{\mathrm{LI}} s_{\mathrm{R}} + w_{\mathrm{R}}) + w_n\right] + \bar{n}_r \\
&= \alpha\left[(\hat{h}_n + \epsilon_n)\sqrt{P_{\mathrm{R}}} A_{\mathrm{R}} \left((\hat{h}_{\mathrm{SR}} + \epsilon_{\mathrm{SR}})\left(\sqrt{P_{\mathrm{S}}} \sum_{n=1}^{N} \sqrt{a_n} x_n\right) + h_{\mathrm{LI}} s_{\mathrm{R}} + w_{\mathrm{R}}\right) + w_n\right] + \bar{n}_r
\end{aligned}
\tag{13}
$$

The users need to perform SIC to obtain the desired signal. The instantaneous signal-to-interference-plus-noise ratio (SINR) of the ith user needed to decode the jth user's signal ($j \leq i$) can be expressed as

$$
\begin{aligned}
\mathrm{SINR}_{i,j} =& \alpha^2 |\hat{h}_i|^2 A_{\mathrm{R}}^2 P_{\mathrm{R}} |\hat{h}_{\mathrm{SR}}|^2 P_{\mathrm{S}} a_j \\
& \times \Bigg(\alpha(|\hat{h}_i|^2 + \sigma_{\mathrm{RU}}^2) A_{\mathrm{R}}^2 P_{\mathrm{R}} (|\hat{h}_{\mathrm{SR}}|^2 + \sigma_{\mathrm{SR}}^2) P_{\mathrm{S}} \\
& - \alpha^2 |\hat{h}_i|^2 A_{\mathrm{R}}^2 P_{\mathrm{R}} |\hat{h}_{\mathrm{SR}}|^2 P_{\mathrm{S}} \sum_{u=1}^{j} a_u \\
& + \alpha(|\hat{h}_i|^2 + \sigma_{\mathrm{RU}}^2) A_{\mathrm{R}}^2 P_{\mathrm{R}} (\ell_{\mathrm{R}} P_{\mathrm{R}} + \sigma_{\mathrm{R}}^2) + \alpha\sigma^2 \Bigg)^{-1}
\end{aligned}
\tag{14}
$$

Here, for user j, the signals to user $\{j+1, \cdots, N\}$ are treated as multiple-access interference signals. We subtract only the power of the signals to user $\{1, \cdots, j\}$ from the total power in the denominator.

The SINR of the ith user necessary to decode the jth user's signal can be denoted by

$$
\mathrm{SINR}_{i,j} = \frac{\alpha a_j \Gamma_1 |\hat{h}_i|^2 |\hat{h}_{\mathrm{SR}}|^2}{b_j \Gamma_1 |\hat{h}_i|^2 |\hat{h}_{\mathrm{SR}}|^2 + \Gamma_2 |\hat{h}_i|^2 + \Gamma_3 |\hat{h}_{\mathrm{SR}}|^2 + \Gamma_4}. \tag{15}
$$

where

$$
\begin{aligned}
\gamma_1 &= P_{\mathrm{S}} / \sigma_{\mathrm{R}}^2 \\
\gamma_2 &= P_{\mathrm{R}} / \sigma_{\mathrm{U}}^2 \\
\gamma_3 &= \beta_{\mathrm{R}} P_{\mathrm{R}} / \sigma_{\mathrm{R}}^2 \\
\Gamma_1 &= \gamma_1 \gamma_2 \\
\Gamma_2 &= \gamma_2 (\sigma_{\mathrm{SR}}^2 \gamma_1 + \gamma_3 + 1) \\
\Gamma_3 &= \gamma_1 (\gamma_2 \sigma_{\mathrm{RU}}^2 + 1) \\
\Gamma_4 &= (\sigma_{\mathrm{RU}}^2 \gamma_2 + 1)(\sigma_{\mathrm{SR}}^2 \gamma_1 + \gamma_3 + 1) \\
b_j &= (1 - \alpha \sum_{u=1}^{j} a_u)
\end{aligned}
\tag{16}
$$

3. Ergodic Rate Analysis

In this section, an analysis of the ergodic rates is presented. Due to the modelling of non-ideal factors, it is very difficult to obtain a closed-form expression for this problem. We obtain an accurate approximation using the theory of mathematical derivations. The ergodic rate for user n can be expressed as

$$C_n = \mathbb{E}\log_2(1+\mathrm{SINR}_{n,n}), \quad n \in N \tag{17}$$

Theorem 1. *The expression for the ergodic rate for user n can be derived as*

$$\begin{aligned} C_n \approx & \sum_{s=0}^{n-1} \frac{N!(-)^s(N-n+s+1)^{-1}}{(n-1)!(N-n)!\ln 2}\binom{n-1}{s} \\ & \times \left[I\left(\frac{\theta_{n,2}}{\theta_{n,1}}, \frac{\theta_{n,3}}{\theta_{n,1}}, \frac{\theta_{n,4}}{\theta_{n,1}}\right) - I\left(\frac{\theta_{n,2}}{\tilde{\theta}_{n,1}}, \frac{\theta_{n,3}}{\tilde{\theta}_{n,1}}, \frac{\theta_{n,4}}{\tilde{\theta}_{n,1}}\right)\right] \end{aligned} \tag{18}$$

where $\theta_{n,1} = (b_n + \alpha a_n)\Gamma_1\beta_{\mathrm{RU}}\beta_{\mathrm{SR}}$, $\tilde{\theta}_{n,1} = b_n\Gamma_1\beta_{\mathrm{RU}}\beta_{\mathrm{SR}}$, $\theta_{n,2} = \beta_{\mathrm{RU}}\Gamma_2$, $\theta_{n,3} = \beta_{\mathrm{SR}}\Gamma_3(N-n+s+1)$ and $\theta_{n,4} = \Gamma_4(N-n+s+1)$. The function $I(\cdot,\cdot,\cdot)$ in (18) is given by

$$\begin{aligned} I(p,q,r) \approx & \, \mathrm{e}^{\frac{r}{q}} E_1\left(\frac{r}{q}\right) + \mathrm{e}^q E_1(q) \\ & + \mathrm{e}^p E_1(p) \sum_{\lambda\in\Lambda}\left\{ h_\lambda \mathrm{e}^{-k_\lambda q}\left[\frac{x_\lambda^2}{2} + \sqrt{x_\lambda} J_1(-2\sqrt{x_\lambda})\right]\right\} \\ & + \sum_{\lambda\in\Lambda}\left\{ h_\lambda \mathrm{e}^{-k_\lambda q}\left[\frac{x^2}{2p} - \sum_{v=2}^{V}\sum_{u=1}^{v-1}\frac{(u-1)!(-)^{v-u}x^v}{v!(v-1)!p^u}\right]\right\}, \end{aligned} \tag{19}$$

where Λ, h_λ, and k_λ are defined in (24), and $x_\lambda = k_\lambda(pq-r)$, $J_1(\cdot)$ denotes the first-order Bessel function of the first kind.

Proof. Through knowledge of order statistics [28], it can be seen that $|\hat{h}_n|^2$ has a density function

$$\begin{aligned} f_n(x) &= \frac{N!\beta_{\mathrm{RU}}^{-1}}{(n-1)!(N-n)!}\left(\mathrm{e}^{-\frac{1}{\beta_{\mathrm{RU}}}x}\right)^{N-n+1}\left(1-\mathrm{e}^{-\frac{1}{\beta_{\mathrm{RU}}}x}\right)^{n-1} \\ &= \frac{N!\beta_{\mathrm{RU}}^{-1}}{(n-1)!(N-n)!}\sum_{s=0}^{n-1}\binom{n-1}{s}(-)^s \mathrm{e}^{-\frac{N-n+s+1}{\beta_{\mathrm{RU}}}x}\mathbf{1}_{(x\geq 0)}, \end{aligned} \tag{20}$$

where $\mathbf{1}_{(\cdot)}$ denotes the indicator function. Using (15), (17), (20), we obtain

$$\begin{aligned} C_n = & \int_0^\infty\int_0^\infty \log_2\left(1+\frac{\alpha a_n\Gamma_1 xy}{b_n\Gamma_1 xy + \Gamma_2 x + \Gamma_3 y + \Gamma_4}\right) \\ & \times f_n(x)\beta_{\mathrm{SR}}^{-1}\mathrm{e}^{-\frac{1}{\beta_{\mathrm{SR}}}y}\,\mathrm{d}x\mathrm{d}y. \end{aligned} \tag{21}$$

Changing variable $x \mapsto (N-n+s+1)\beta_{\mathrm{RU}}^{-1}x$ and $y \mapsto \beta_{\mathrm{SR}}^{-1}y$, (20) can be expressed as

$$\begin{aligned} C_n = & \sum_{s=0}^{n-1}\frac{N!(-)^s(N-n+s+1)^{-1}}{(n-1)!(N-n)!\ln 2}\binom{n-1}{s} \\ & \times \int_0^\infty\int_0^\infty \ln\left(\frac{\theta_{n,1}xy+\theta_{n,2}x+\theta_{n,3}y+\theta_{n,4}}{\tilde{\theta}_{n,1}xy+\theta_{n,2}x+\theta_{n,3}y+\theta_{n,4}}\right)\mathrm{e}^{-x-y}\,\mathrm{d}x\mathrm{d}y. \end{aligned} \tag{22}$$

We could carry on calculating the integral in (22) as follows:

$$\begin{aligned} I(p,q,r) &= \int_0^\infty\int_0^\infty \ln(xy+px+qy+r)\mathrm{e}^{-x-y}\,\mathrm{d}x\mathrm{d}y - \ln r \\ &= \int_0^{+\infty}\left[\ln\left(\frac{q}{r}y+1\right) + \mathrm{e}^{\frac{qy+r}{y+p}}E_1\left(\frac{qy+r}{y+p}\right)\right]\mathrm{e}^{-y}\,\mathrm{d}y \\ &\approx \mathrm{e}^{\frac{r}{q}}E_1\left(\frac{r}{q}\right) + \int_0^{+\infty}\sum_{\lambda\in\Lambda}h_\lambda \mathrm{e}^{-k_\lambda\frac{qy+r}{y+p}}\mathrm{e}^{-y}\,\mathrm{d}y \end{aligned} \tag{23}$$

where we used an approximation of $E_1(\cdot)$ in [29]

$$\mathrm{e}^{s}E_1(s) \approx \sum_{\lambda\in\Lambda} h_\lambda \mathrm{e}^{-k_\lambda s}, \tag{24}$$

where $\Lambda = \{\lambda = (u,v) \in \mathbb{N}^2 : 1 \le u \le \tilde{U}+1, 1 \le v \le \tilde{V}+1\}$, and

$$h_\lambda = 4\sqrt{2}\pi\phi_u\phi_v\sqrt{\chi_u}, \quad k_\lambda = 1 - 4\chi_u\chi_v, \quad \lambda = (u,v). \tag{25}$$

Here, the parameters $\phi_j = (\theta_j - \theta_{j-1})/\pi \ge 0$ and $\chi_j = \frac{1}{2}\frac{\cot(\theta_{j-1})-\cot(\theta_j)}{\theta_j-\theta_{j-1}} \ge 1/2$.

The integrand of the last integral in Equation (23) can be estimated using a Taylor series, as follows:

$$\sum_{\lambda\in\Lambda} h_\lambda \mathrm{e}^{-k_\lambda \frac{qy+r}{y+p}}\mathrm{e}^{-y} \approx \sum_{\lambda\in\Lambda} h_\lambda \mathrm{e}^{-k_\lambda q}\sum_{v=0}^{V}\frac{k_\lambda^v (pq-r)^v}{v!(y+p)^v}\mathrm{e}^{-y}. \tag{26}$$

Using the above results and Equation (3.353.2) in [30], (19) is proved. Hence, the proof of the theorem is completed. □

4. Outage Probability Analysis

We define the outage event $A_{i,j} = \{\mathrm{SINR}_{i,j} \le \gamma_{\mathrm{th}j}\}$, where $\gamma_{\mathrm{th}j}$ is the target threshold for the jth user. Then, event $A_{i,j}^c$ means that the ith user cannot decode the jth user's signal. An outage occurs for the ith user when any of $A_{i,j}^c$ occurs. The probability of an outage for the ith user can be expressed as

$$\mathcal{P}_{\mathrm{out}}^i = \Pr\left(\bigcup_{j=1}^{i} A_{i,j}^c\right) = 1 - \Pr(A_{i,1}\cdots A_{i,i}). \tag{27}$$

Theorem 2. *A closed-form expression of the probability of an outage for user i ($\mathcal{P}_{\mathrm{out}}^i$) can be obtained as*

$$\begin{aligned}\mathcal{P}_{\mathrm{out}}^i = 1 - \frac{N!\beta_{\mathrm{RU}}^{-1}}{(i-1)!(N-i)!}\sum_{s=0}^{i-1} 2\binom{i-1}{s}(-1)^s \mathrm{e}^{-\left(\frac{\Gamma_2\delta_i^\star}{\beta_{\mathrm{SR}}\Gamma_3}+\chi_{i,s}\delta_i^\star\right)} \\ \times\sqrt{\frac{\phi_i}{\chi_{i,s}}}\mathrm{K}_1\left(2\sqrt{\phi_i\chi_{i,s}}\right)\end{aligned} \tag{28}$$

where $\chi_{i,s}$, ϕ_i, and $\delta_i^\star$ are defined in (32), and $\mathrm{K}_1(\cdot)$ denotes the first-order modified Bessel function of the second kind.

Proof. By replacing (15) in $A_{i,j}$, it can be rewritten as

$$A_{i,j} = \left\{|\hat{h}_i|^2 \ge \delta_j, |\hat{h}_{\mathrm{SR}}|^2 \ge \frac{(\Gamma_2|\hat{h}_i|^2+\Gamma_4)\delta_j}{\Gamma_3(|\hat{h}_i|^2-\delta_j)}\right\}, \tag{29}$$

where $\delta_j := \frac{\gamma_{\mathrm{th}j}\Gamma_3}{\Gamma_1(\alpha a_j - b_j\gamma_{\mathrm{th}j})}$. By noting that $\delta_j/(|\hat{h}_i|^2-\delta_j)$ is monotone in δ_j, we can obtain that

$$A_{i,1}\cdots A_{i,i} = \left\{|\hat{h}_i|^2 \ge \delta_i^\star, |\hat{h}_{\mathrm{SR}}|^2 \ge \frac{(\Gamma_2|\hat{h}_i|^2+\Gamma_4)\delta_i^\star}{\Gamma_3(|\hat{h}_i|^2-\delta_i^\star)}\right\}, \tag{30}$$

where $\delta_i^\star = \max(\delta_1,\cdots,\delta_i)$.

Hence, $\mathcal{P}_{\text{out}}^{i}$ can be denoted as

$$\begin{aligned}\mathcal{P}_{\text{out}}^{i} &= 1 - \Pr(A_{i,1} \cdots A_{i,i}) \\ &= 1 - \int_{\delta_i^\star}^{\infty} f_i(y) \int_{\frac{(\Gamma_2 y + \Gamma_4)\delta_i^\star}{\Gamma_3(y-\delta_i^\star)}}^{\infty} \mathrm{d}F_{|\hat{h}_{\text{SR}}|^2}(x)\mathrm{d}y \\ &= 1 - \frac{N!\beta_{\text{RU}}^{-1}\mathrm{e}^{-\frac{\Gamma_2\delta_i^\star}{\beta_{\text{SR}}\Gamma_3}}}{(i-1)!(N-i)!}\sum_{s=0}^{i-1}\binom{i-1}{s}(-1)^s\int_{\delta_i^\star}^{\infty}\mathrm{e}^{-\left(\chi_{i,s}y+\frac{\phi_i}{y-\delta_i^\star}\right)}\mathrm{d}y,\end{aligned} \tag{31}$$

where

$$\chi_{i,s} = \frac{N-i+s+1}{\beta_{\text{RU}}}, \quad \phi_i = \frac{\delta_i^\star(\Gamma_4 + \delta_i^\star\Gamma_2)}{\beta_{\text{SR}}\Gamma_3}. \tag{32}$$

It follows from (3.471.9) in [30] that (28) holds, and hence, the proof of the theorem is completed. □

5. Numerical Results

In this section, numerical results are provided to verify the correctness of the theoretical results in Sections 3 and 4. Additionally, we use these results to analyze the impact of the following parameter variations on the system performance, such as transmission power, transmission phases, LI levels, channel estimation error levels, and quantization bits of the ADCs. For all simulations, $\beta_{\text{SR}} = 0.4$, $\beta_{\text{RU}} = 0.6$, and the power allocation coefficients $= [\frac{1}{2}, \frac{1}{3}, \frac{1}{6}]$.

Figures 3 and 4 plot the outage probability and ergodic rate versus the SNR in the first phase (γ_1) with *cee* $= 0.001$, $\beta_{\text{LI}} = 0.005$, $\gamma_2 = 20$ dB, quantization bits $= 6$, and $\gamma_{\text{th}} = [0.1, 0.1, 0.1]$ dB. Figures 5 and 6 plot the outage probability and ergodic rate versus the SNR in the second phase (γ_2) with *cee* $= 0.001$, $\beta_{\text{LI}} = 0.005$, $\gamma_1 = 30$ dB, quantization bits $= 6$, and $\gamma_{\text{th}} = [0.1, 0.1, 0.1]$ dB. Figures 7 and 8 plot the outage probability and ergodic rate versus different loopback interference levels (β_{LI}) with *cee* $= 0.001$, $\gamma_1 = 30$ dB, $\gamma_2 = 20$ dB, quantization bits $= 6$, and $\gamma_{\text{th}} = [0.1, 0.1, 0.1]$ dB. Figures 9 and 10 plot the outage probability and ergodic rate versus different channel estimation error levels and quantization bits with $\beta_{\text{LI}} = 0.005$, $\gamma_1 = 30$ dB, and $\gamma_2 = 20$ dB.

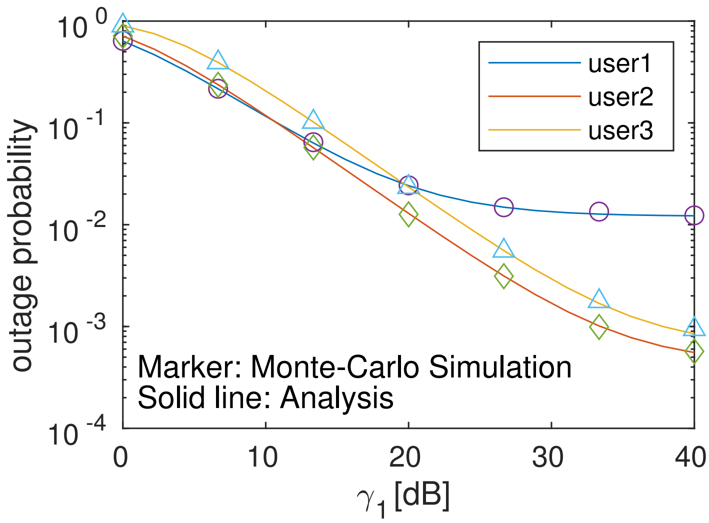

Figure 3. Outage probability versus SNR in the first phase (γ_1) with *cee* $= 0.001$, $\beta_{\text{LI}} = 0.005$, $\beta_{\text{SR}} = 0.4$, $\beta_{\text{RU}} = 0.6$, $\gamma_2 = 20$ dB, quantization bits $= 6$, power allocation coefficients $= [\frac{1}{2}, \frac{1}{3}, \frac{1}{6}]$, and $\gamma_{\text{th}} = [0.1, 0.1, 0.1]$ dB.

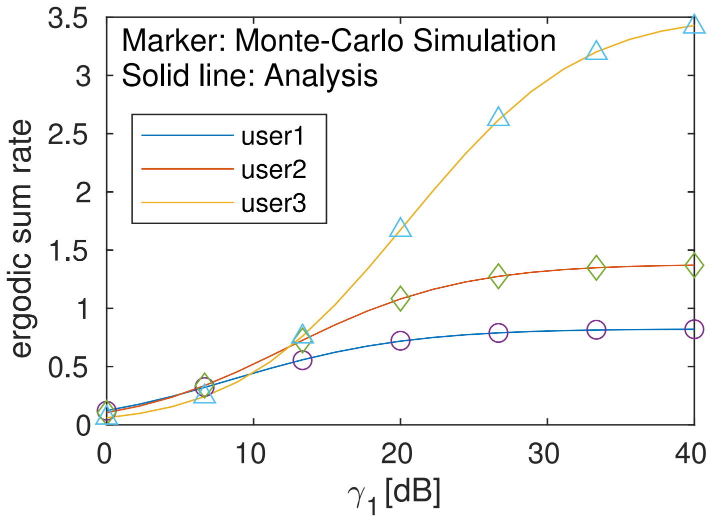

Figure 4. Ergodic rates versus SNR in the first phase (γ_1) with $cee = 0.001$, $\beta_{\text{LI}} = 0.005$, $\beta_{\text{SR}} = 0.4$, $\beta_{\text{RU}} = 0.6$, $\gamma_2 = 20$ dB, quantization bits = 6, and power allocation coefficients = $[\frac{1}{2}, \frac{1}{3}, \frac{1}{6}]$.

From Figures 3 and 4, it can be seen that when the transmission power of the second stage is fixed, the outage probability gradually decreases, and the ergodic rate gradually increases as the transmission power of the first stage is increased. For different users, the obtained results have shown the existence of a floor at moderate and high SNR levels, which is due to channel estimation errors and residual LI. It is also noted that both the outage probability and ergodic rate of user 3 outperforms user 2 and user 1. User 1 has the worst performance. This happens because NOMA assigns the largest power factor to the user with the worst channel conditions, so the first user has the highest outage probability and the lowest ergodic rate. Figures 5 and 6 show the effect of transmit power variation on the outage probability and ergodic rate of the system in the second transmission stage. The performance improves as the transmit power increases under moderate or high SNRs. For both the outage probability and ergodic rate, there are SNR boundaries corresponding to maximum points of curves. The performance decreases for all users when the SNR increases over boundaries. This is because the SINR of the relay is dominated by a large residual LBI.

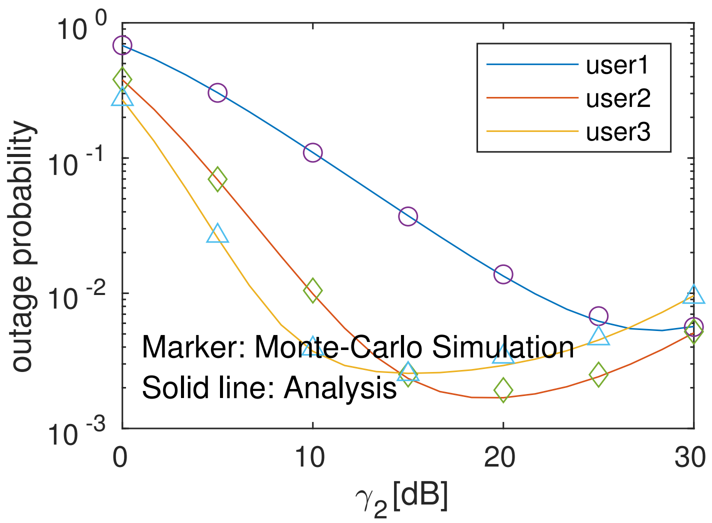

Figure 5. Outage probability versus SNR in the second phase (γ_2) with $cee = 0.001$, $\beta_{\text{LI}} = 0.005$, $\beta_{\text{SR}} = 0.4$, $\beta_{\text{RU}} = 0.6$, $\gamma_1 = 30$ dB, quantization bits = 6, power allocation coefficients = $[\frac{1}{2}, \frac{1}{3}, \frac{1}{6}]$, and $\gamma_{\text{th}} = [0.1, 0.1, 0.1]$ dB.

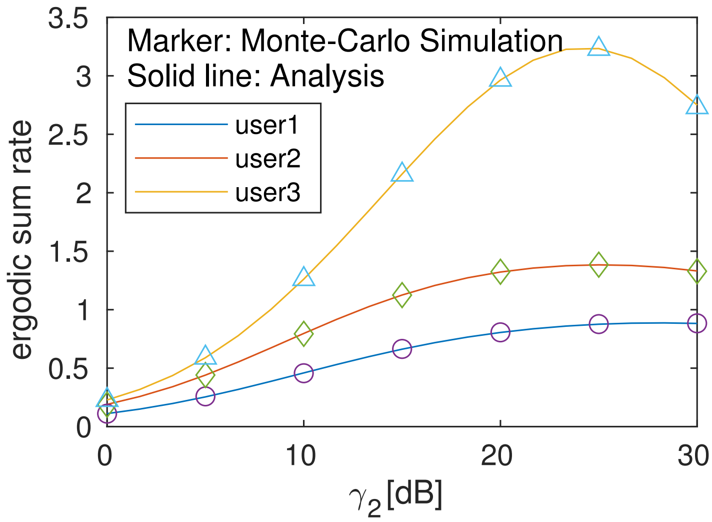

Figure 6. Ergodic rates versus SNR in the second phase (γ_2) with $cee = 0.001$, $\beta_{\text{LI}} = 0.005$, $\beta_{\text{SR}} = 0.4$, $\beta_{\text{RU}} = 0.6$, $\gamma_1 = 30$ dB, quantization bits = 6, and power allocation coefficients = $[\frac{1}{2}, \frac{1}{3}, \frac{1}{6}]$.

Figures 7 and 8 show the experimental results on the effect of LI gain level on the system performance. It is obvious to see that as the LI gain increases, the performance of the system progressively deteriorates, which is shown in the figures as an increase in the outage probability and a decrease in the ergodic rate. This is due to the higher interference level, which makes the signal relatively smaller. Therefore, a practical transceiver design would adopt a combination of the RF domain, analog domain, and digital domain's self-interference cancellations to mitigate LI. If it is hard to ensure that LI is suppressed within an acceptable range, it is better to use HD mode.

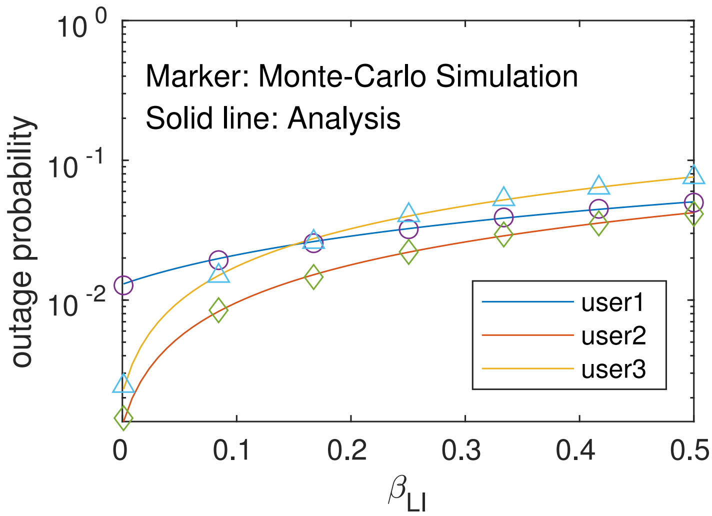

Figure 7. Outage probability versus different loopback interference levels (β_{LI}) with $cee = 0.001$, $\beta_{\text{SR}} = 0.4$, $\beta_{\text{RU}} = 0.6$, $\gamma_1 = 30$ dB, $\gamma_2 = 20$ dB, quantization bits = 6, power allocation coefficients = $[\frac{1}{2}, \frac{1}{3}, \frac{1}{6}]$, and $\gamma_{\text{th}} = [0.1, 0.1, 0.1]$ dB.

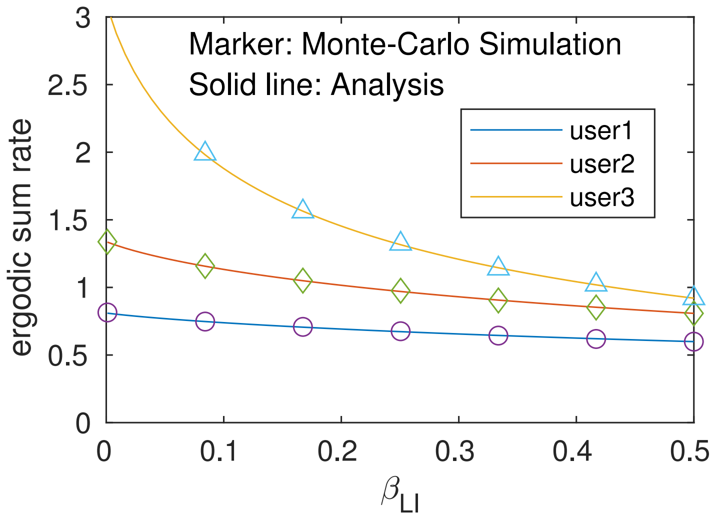

Figure 8. Ergodic rates versus different loopback interference levels (β_{LI}) with $cee = 0.001$, $\beta_{\mathrm{SR}} = 0.4$, $\beta_{\mathrm{RU}} = 0.6$, $\gamma_1 = 30$ dB, $\gamma_2 = 20$ dB, quantization bits $= 6$, and power allocation coefficients $= [\frac{1}{2}, \frac{1}{3}, \frac{1}{6}]$.

Finally, the effect of quantization bits of the low-resolution ADC on the outage probability and ergodic rate is illustrated in Figures 9 and 10. It can be seen that both the outage and ergodic rate performances are degraded by higher channel estimation errors. Channel estimation errors also lead to a floor in high SNR areas. When the quantization bits of the ADC are very low, the system performance is poor even if the channel estimation error is small. It can be observed that the outage and ergodic rate gradually improve as the number of quantization bits increases from 1 to 6. However, there is no significant performance gain as the number of quantization bits continues to increase. Instead, performance can be improved by reducing the strength of the loopback interference. This result provides insight for system design, as appropriate quantization bits can be chosen to achieve the desired resolution and balance device cost and performance enhancement benefits.

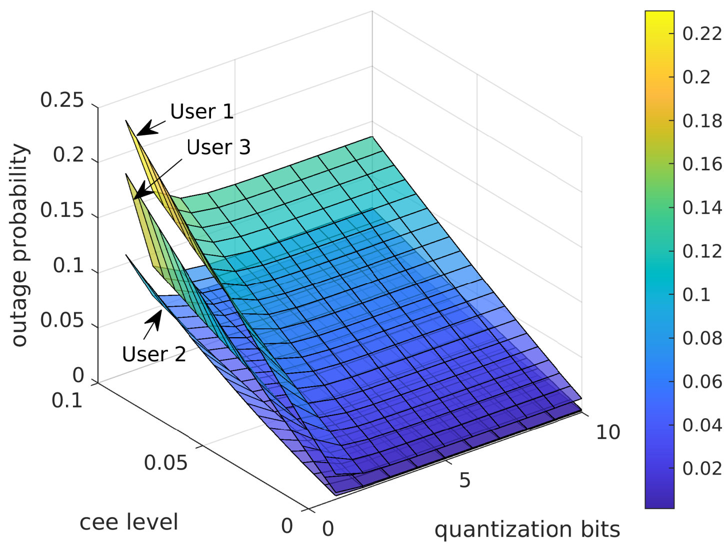

Figure 9. Outage probability versus channel estimation error level and quantization bits with $\beta_{\mathrm{LI}} = 0.005$, $\beta_{\mathrm{SR}} = 0.4$, $\beta_{\mathrm{RU}} = 0.6$, $\gamma_1 = 30$ dB, $\gamma_2 = 20$ dB, power allocation coefficients $= [\frac{1}{2}, \frac{1}{3}, \frac{1}{6}]$, and $\gamma_{\mathrm{th}} = [0.1, 0.1, 0.1]$ dB.

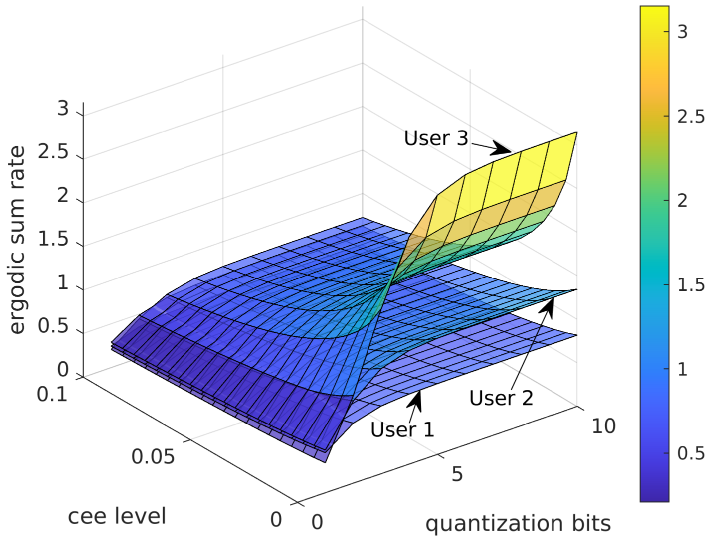

Figure 10. Ergodic rates versus different channel estimation error levels and quantization bits with $\beta_{\mathrm{LI}} = 0.005$, $\beta_{\mathrm{SR}} = 0.4$, $\beta_{\mathrm{RU}} = 0.6$, $\gamma_1 = 30$ dB, $\gamma_2 = 20$ dB, and power allocation coefficients $= [\frac{1}{2}, \frac{1}{3}, \frac{1}{6}]$.

6. Conclusions

In this paper, we have proposed an FD C-NOMA system where the BS serves multiple geographically separated users over the downlink. All users receive the information with the assistance of a FD relay node. The performance of this FD C-NOMA multi-user system is analyzed by considering the impact of channel estimation errors, the resiual LI, and low-resolution ADC. Furthermore, an accurate approximate expression of the ergodic rate and a closed-form expression of the outage probability for each user are presented. The accuracy of each theoretical result was verified by Monte Carlo simulations. The obtained results have shown that the performance is influenced by the LI level, channel estimation error, and the quantization bits in ADC. Both the outage and ergodic rate performance encounter floors caused by high channel estimation errors and LI. Moreover, the FD C-NOMA mode is degraded at high SNRs due to a high residual LI. It also can be observed that the outage and ergodic rate improve as the number of quantization bits increases. However, the performance improvement tends to flatten out as quantization bits continue to increase.

Author Contributions: Investigation, methodology, and supervision, S.W.; simulation and validation, Y.H.; conceptualization and formal analysis, Y.Y.; writing—original draft preparation and visualization, Y.H. and Y.Y.; writing—review and editing, S.W. All authors have read and agreed to the published version of the manuscript.

Funding: This paper is supported by National Natural Science Foundation of China (Grant 61971061) and Beijing Natural Science Foundation (Grant L223026).

Institutional Review Board Statement: Not applicable.

Informed Consent Statement: Not applicable.

Data Availability Statement: Not applicable.

Acknowledgments: This work is conducted in Information Theory and Technology Center (ITTC) of Beijing University of Posts and Telecommunications. The authors would like to thank the reviewers for several insightful comments and suggestions which helped us to improved the paper.

Conflicts of Interest: The authors declare no conflict of interest.

Abbreviations

The following abbreviations are used in this manuscript:

ADCs	Analog-to-digital converters
AF	Amplify-and-forward
BER	Bit error rate
BS	Base station
cdf	Cumulative (probability measure) distribution function
CDMA	Code division multiple access
CSI	Channel state information
C-NOMA	Cooperative NOMA
ch.f.	Characteristic function
CSI	Channel state information
DF	Decode-and-forward
ER	Ergodic rate
FD	Full duplex
FDMA	Frequency division multiple access
HD	Half duplex
i.i.d.	Independent and identically distributed
LI	Loopback interference
NOMA	Non-orthogonal multiple access
OFDMA	Orthogonal frequency division multiple access
OMA	Orthogonal multiple access
OP	Outage probability
Qos	Quality of service
pdf	Probability density function
RF	Radio frequency
r.v.	Random variable
SER	Symbol error rate
SIC	Successive interference cancellation
SINR	Signal-to-interference-plus-noise ratio
SNR	Signal-to-noise ratio
TDMA	Time division multiple access
UE	User equipment

References

1. Liu, Y.; Zhang, S.; Mu, X.; Ding, Z.; Schober, R.; Al-Dhahir, N.; Hossain, E.; Shen, X. Evolution of NOMA toward Next Generation Multiple Access (NGMA) for 6G. *IEEE J. Sel. Areas Commun.* **2022**, *40*, 1037–1071. [CrossRef]
2. Zhang, Z.; Yang, G.; Ma, Z.; Xiao, M.; Ding, Z.; Fan, P. Heterogeneous ultradense networks with NOMA: System architecture, coordination framework, and performance evaluation. *IEEE Veh. Technol. Mag.* **2018**, *13*, 110–120. [CrossRef]
3. Dai, L.; Wang, B.; Ding, Z.; Wang, Z.; Chen, S.; Hanzo, L. A survey of non-orthogonal multiple access for 5G. *IEEE Commun. Surv. Tutor.* **2018**, *20*, 2294–2323. [CrossRef]
4. Men, J.; Ge, J. Non-orthogonal multiple access for multiple-antenna relaying networks. *IEEE Commun. Lett.* **2015**, *19*, 1686–1689. [CrossRef]
5. So, J.; Sung, Y. Improving non-orthogonal multiple access by forming relaying broadcast channels. *IEEE Commun. Lett.* **2016**, *20*, 1816–1819. [CrossRef]
6. Jiao, R.; Dai, L.; Zhang, J.; MacKenzie, R.; Hao, M. On the Performance of NOMA-Based Cooperative Relaying Systems Over Rician Fading Channels. *IEEE Trans. Veh. Technol.* **2017**, *66*, 11409–11413. [CrossRef]
7. Choi, J.I.; Jain, M.; Srinivasan, K.; Levis, P.; Katti, S. Achieving single channel, full duplex wireless communication. In Proceedings of the 16th Annual International Conference on Mobile Computing and Networking, Chicago, IL, USA, 20–24 September 2010; pp. 1–12.
8. Duarte, M.; Dick, C.; Sabharwal, A. Experiment-driven characterization of full-duplex wireless Systems. *IEEE Trans. Wirel. Commun.* **2012**, *11*, 4296–4307. [CrossRef]
9. Sabharwal, A.; Schniter, P.; Guo, D.; Bliss, D.W.; Rangarajan, S.; Wichman, R. In-Band Full-Duplex Wireless: Challenges and Opportunities. *IEEE J. Sel. Areas Commun.* **2014**, *32*, 1637–1652. [CrossRef]
10. Heino, M.; Korpi, D.; Huusari, T.; Rodríguez, E.A.; Venkatasubramanian, S.; Riihonen, T.; Anttila, L.; Icheln, C.; Haneda, K.; Wichman, R.; et al. Recent advances in antenna design and interference cancellation algorithms for in-band full duplex relays. *IEEE Commun. Mag.* **2015**, *53*, 91–101. [CrossRef]

11. Korpi, D.; Tamminen, J.; Turunen, M.; Huusari, T.; Choi, Y.; Anttila, L.; Talwar, S.; Valkama, M. Full-Duplex Mobile Device: Pushing the Limits. *IEEE Commun. Mag.* **2016**, *54*, 80–87. [CrossRef]
12. Zhang, Z.; Ma, Z.; Xiao, M.; Ding, Z.; Fan, P. Full-duplex device-to-device-aided cooperative nonorthogonal multiple access. *IEEE Trans. Veh. Technol.* **2017**, *66*, 4467–4471.
13. Zhong, C.; Zhang, Z. Non-orthogonal multiple access with cooperative full-duplex relaying. *IEEE Commun. Lett.* **2016**, *20*, 2478–2481. [CrossRef]
14. Zhang, L.; Liu, J.; Xiao, M.; Wu, G.; Liang, Y.C.; Li, S. Performance analysis and optimization in downlink NOMA systems with cooperative full-duplex relaying. *IEEE J. Sel. Areas Commun.* **2017**, *35*, 2398–2412. [CrossRef]
15. Wang, X.; Jia, M.; Ho, I.W.H.; Guo, Q.; Lau, F.C.M. Exploiting Full-Duplex Two-Way Relay Cooperative Non-Orthogonal Multiple Access. *IEEE Trans. Commun.* **2019**, *67*, 2478–2481. [CrossRef]
16. Kong, C.; Zhong, C.; Jin, S.; Yang, S.; Lin, H.; Zhang, Z. Full-Duplex Massive MIMO Relaying Systems with Low-Resolution ADCs. *IEEE Trans. Wirel. Commun.* **2017**, *16*, 5033–5047. [CrossRef]
17. Wang, D.; Wang, S. Outage Performance for full-duplex decode-and-forward relay Cooperative Networks with low-resolution ADCs. In Proceedings of the 2018 IEEE/CIC International Conference on Communications in China (ICCC), Beijing, China, 16–18 August 2018.
18. Liu, Z.; Zhang, L.; Ding, Z. Overcoming the Channel Estimation Barrier in Massive MIMO Communication via Deep Learning. *IEEE Wirel. Commun.* **2020**, *27*, 104–111. [CrossRef]
19. Wang, S.; Li, Y.; Wang, M.; Xu, W. Performance comparison of in-band full-duplex and half-duplex two-hop relaying with channel estimation errors. *IEICE Trans. Commun.* **2018**, *E101-B*, 573–581. [CrossRef]
20. Wang, S.; Wang, D.; Li, C.; Xu, W. Full Duplex AF and DF Relaying Under Channel Estimation Errors for V2V Communications. *IEEE Access* **2018**, *6*, 65321–65332. [CrossRef]
21. Aswathi, V.; Babu, A.V. Full/half duplex cooperative NOMA under imperfect successive interference cancellation and channel state estimation errors. *IEEE Access* **2019**, *7*, 179961–179984. [CrossRef]
22. Le, N.P.; Le, K. Uplink NOMA Short-Packet Communications with Residual Hardware Impairments and Channel Estimation Errors. *IEEE Trans. Veh. Technol.* **2022**, *71*, 4057–4072. [CrossRef]
23. Chu, T.; Zepernick, H.J. Performance of a Non-Orthogonal Multiple Access System with Full-Duplex Relaying. *IEEE Commun. Lett.* **2018**, *22*, 2084–2087. [CrossRef]
24. Aswathi, V.; Babu, A.V. Outage and Throughput Analysis of Full-Duplex Cooperative NOMA System with Energy Harvesting. *IEEE Trans. Veh. Technol.* **2021**, *70*, 11648–11664. [CrossRef]
25. Xu, B.; Xiang, Z.; Ren, P.; Guo, X. Outage Performance of Downlink Full-Duplex Network-Coded Cooperative NOMA. *IEEE Wirel. Commun. Lett.* **2021**, *10*, 26–29. [CrossRef]
26. Senthilkumar, D.; Chitra, M. Performance Analysis of NOMA in Full-Duplex Cooperative Spectrum Sharing Systems. *IEEE Trans. Veh. Technol.* **2022**, *71*, 9095–9100.
27. Li, W.; Liu, M.; Deng, C.; Mathiopoulos, P.T.; Ding, Z.; Liu, Y. Full-Duplex Cooperative NOMA Relaying Systems With I/Q Imbalance and Imperfect SIC. *IEEE Wirel. Commun. Lett.* **2020**, *9*, 17–20. [CrossRef]
28. Devore, J.L.; Berk, K.N.; Carlton, M.A. *Modern Mathematical Statistics with Applications*; Springer: Berlin/Heidelberg, Germany, 2012; Volume 285.
29. Alkheir, A.; Ibnkahla, M. An accurate approximation of the exponential integral function using a sum of exponentials. *IEEE Commun. Lett.* **2013**, *17*, 1364–1367. [CrossRef]
30. Gradshteyn, I.S.; Ryzhik, I.M. *Tables of Integrals, Series, and Products*, 8th ed.; Academic Press: Cambridge, MA, USA, 2015.